Monthly Notices
of the
ROYAL ASTRONOMICAL SOCIETY

MNRAS **448,** 1372–1377 (2015) doi:10.1093/mnras/stu2602

Infrared spectra and chemical abundance of methyl propionate in icy astrochemical conditions

B. Sivaraman,[1*] N. Radhika,[2] A. Das,[3] G. Gopakumar,[2,4] L. Majumdar,[3] S. K. Chakrabarti,[3,5] K. P. Subramanian,[1] B. N. Raja Sekhar[6] and M. Hada[2,4]

[1]*Space and Atmospheric Sciences Division, Physical Research Laboratory, Ahmedabad 380 009, India*
[2]*Department of Chemistry, Tokyo Metropolitan University, 1-1 Minami-Osawa, Hachioji, Tokyo 192-0397, Japan*
[3]*Indian Centre for Space Physics, 43 Chalantika, Garia Station Road, Kolkata 700084, India*
[4]*JST, CREST, 4-1-8 Honcho, Kawaguchi, Saitama 332-0012, Japan*
[5]*S. N. Bose National Centre for Basic Sciences, Salt Lake, Kolkata 700098, India*
[6]*B-4, Indus-1, BARC Spectroscopy Lab at Indus-1, Atomic and Molecular Physics Division, BARC, Mumbai & RRCAT, Indore 452013, India*

Accepted 2014 December 3. Received 2014 December 2; in original form 2014 September 22

ABSTRACT

We carried out an experiment in order to obtain the infrared (IR) spectra of methyl propionate ($CH_3CH_2COOCH_3$) in astrochemical conditions and present the IR spectra for future identification of this molecule in the interstellar medium (ISM). The experimental IR spectrum is compared with the theoretical spectrum, and an attempt was made to assign the observed peak positions to their corresponding molecular vibrations in condensed phase. Moreover, our calculations suggest that methyl propionate must be synthesized efficiently within the complex chemical network of the ISM and therefore be present in cold dust grains, awaiting identification.

Key words: astrochemistry – methods: laboratory: molecular – ISM: abundances – ISM: molecules – infrared: general.

INTRODUCTION

The identification of methyl acetate (CH_3COOCH_3) in the interstellar medium (ISM; Tercero et al. 2013) implied the presence of propionic acid (CH_3CH_2COOH) in similar regions where methyl acetate was detected. Methyl acetate dissociation carried out experimentally simulating the interstellar cold conditions also pointed out the formation of alcohol, methyl alcohol (CH_3OH), along with other products to form from acetate (Sivaraman et al. 2014). In interstellar chemistry, methyl alcohol is among the most dominant molecule influencing various chemical reactions that takes place on cold dust grains. In methyl acetate dominant regions, there are strong chances of propionic acid to be present (Karton & Talbi 2014). The addition of methyl alcohol may lead to the next generation of molecule that can form from the reaction of propionic acid and methyl alcohol, which on the surface of a cold dust grain can lead to the formation of methyl propionate ($CH_3CH_2COOCH_3$) molecule (equation 1). However, there are no experimental IR spectra available in the literature for methyl propionate at conditions commensurate to cold ISM environment. Therefore, here we present the first experimental IR spectra, along with the theoretical spectra, of methyl propionate that will help in the identification of methyl propionate in various regions of the ISM where methyl propionate must be component as shown by our gas-grain chemical model.

$$CH_3OH + CH_3CH_2COOH \rightarrow CH_3CH_2COOCH_3 + H_2O \quad (1)$$

METHODS AND THEORETICAL DETAILS

Experimental method

Experiments were carried out in the low-temperature astrochemistry apparatus housed in the Physical Research Laboratory (PRL); a detailed description of the experimental apparatus can be found elsewhere (Sivaraman et al. 2014). Upon achieving ultrahigh vacuum of the order of 10^{-9} mbar and low temperature (85 K) at the zinc selenide (ZnSe) substrate, methyl propionate molecules in the gas phase, extracted from the liquid sample that was freeze–pump–thawed three times to eliminate any impurity, were let into the chamber to form icy layers of methyl propionate at 85 K. Sample deposition was monitored by Fourier Transform Infrared spectrometer operated in the mid-infrared wavelength, 4000–400 cm^{-1}. Absorbance scale in the spectra recorded while depositing the sample was used as an indicator to cease the deposition; in this case, absorbance was kept less than 1.

* E-mail. bhala@prl.res.in

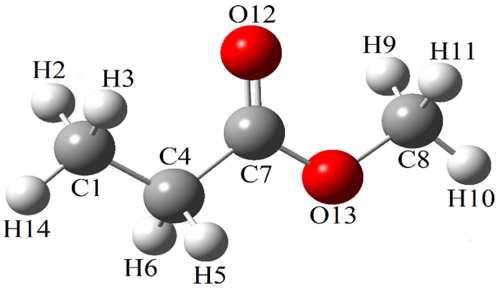

Figure 1. Structure of methyl propionate at equilibrium geometry at MP2 level.

Computational details

The electronic structure calculations were performed using GAUSSIAN 09 software package (Frisch et al. 2009). The optimization of molecular geometry and the IR frequency analysis were first carried out at ab initio MP2 (second-order Möller–Plesset theory) level (Møller & Plesset 1934). To determine the accuracy of the ab initio calculation, we also performed the vibrational analysis using DFT B3LYP (Becke 1988; Lee, Yang & Parr 1988; Stephens et al. 1994) and PBEPBE (Perdew, Burke & Ernzerhof 1996) functional. All the calculations were performed using the Dunning's correlation consistent basis set cc-pVTZ (Woon & Dunning 1993).

For all the 36 vibrational modes, harmonic and anharmonic frequencies with their corresponding infrared intensities have been computed at DFT as well as MP2 levels of theory using the algorithms implemented in GAUSSIAN 09.

RESULTS AND DISCUSSION

To the best of our knowledge, there were no X-ray crystallographic data available for methyl propionate molecule. Hence, we modelled the molecule in gas phase (Fig. 1) and obtained the structural parameters. The bond length, bond angle and dihedral angle are tabulated in Table 1. Comparing different methods, we find bond lengths to be shorter for MP2 in comparison with the DFT calculations. The bond angles and dihedral angles are found to be similar in both the methods. As methyl propionate can be formed from methyl alcohol and propionic acid as given in equation (1), we compared the trend in structural parameters among these molecules. The C—H, C—C and C—O bonds were found to be differing by 0.13, 0.01 and 0.04 Å, respectively (Venkateswarlu & Gordy 1955; Strieter et al. 1962). The C=O bond length varies only by 0.02 Å. Further, the bond

Table 1. Structural parameters of methyl propionate at the DFT-PBEPBE, DFT-B3LYP and MP2 level of theory.

Method	PBEPBE		B3LYP		MP2	
			Bond length (Å)			
	C1—C4	1.5242	C1—C4	1.5228	C1—C4	1.5180
	C1—H2	1.0973	C1—H2	1.0891	C1—H2	1.0871
	C1—H3	1.0973	C1—H3	1.0891	C1—H3	1.0871
	C1—H14	1.0979	C1—H14	1.0900	C1—H14	1.0877
	C4—C7	1.5146	C4—C7	1.5117	C4—C7	1.5055
	C4—H5	1.1014	C4—H5	1.0926	C4—H5	1.0903
	C4—H6	1.1014	C4—H6	1.0927	C4—H6	1.0903
	C7—O12	1.2152	C7—O12	1.2049	C7—O12	1.2106
	C7—O13	1.3624	C7—O13	1.3503	C7—O13	1.3501
	C8—O13	1.4424	C8—O13	1.4362	C8—O13	1.4335
	C8—H9	1.0978	C8—H9	1.0887	C8—H9	1.0867
	C8—H10	1.0978	C8—H10	1.0887	C8—H10	1.0836
	C8—H11	1.0944	C8—H11	1.0857	C8—H11	1.0867
			Bond angle (°)			
	C1—C4—C7	113.0	C1—C4—C7	113.2	C1—C4—C7	112.2
	H2—C1—C4	111.0	H2—C1—C4	111.1	H2—C1—C4	110.8
	H3—C1—C4	111.0	H3—C1—C4	111.1	H3—C1—C4	110.8
	H14—C1—C4	110.6	H14—C1—C4	110.4	H14—C1—C4	110.5
	C4—C7—O12	125.9	C4—C7—O12	125.8	C4—C7—O12	125.8
	C4—C7—O13	110.6	C4—C7—O13	110.9	C4—C7—O13	110.8
	H5—C4—C1	111.6	H5—C4—C1	111.4	H5—C4—C1	111.7
	H6—C4—C1	111.6	H6—C4—C1	111.4	H6—C4—C1	111.7
	C7—O13—C8	114.6	C7—O13—C8	115.8	C7—O13—C8	113.9
	H9—C8—O13	110.6	H9—C8—O13	110.6	H9—C8—O13	110.5
	H10—C8—O13	105.6	H10—C8—O13	105.7	H10—C8—O13	105.6
	H11—C8—O13	110.6	H11—C8—O13	110.6	H11—C8—O13	110.5
			Dihedral angle (°)			
	C1—C4—C7—O13	179.9	C1—C4—C7—O13	179.9	C1—C4—C7—O13	180.0
	C8—O13—C7—C4	180.0	C8—O13—C7—C4	180.0	C8—O13—C7—C4	180.0
	H2—C1—C4—C7	59.7	H2—C1—C4—C7	59.8	H2—C1—C4—C7	59.6
	H3—C1—C4—C7	– 59.6	H3—C1—C4—C7	– 59.7	H3—C1—C4—C7	– 59.5
	H14—C1—C4—C7	– 179.9	H14—C1—C4—C7	– 179.9	H14—C1—C4—C7	– 180.0
	H9—C8—O13—C7	– 60.3	H9—C8—O13—C7	– 60.4	H9—C8—O13—C7	– 60.3
	H10—C8—O13—C7	180.0	H10—C8—O13—C7	180.0	H10—C8—O13—C7	180.0
	H11—C8—O13—C7	60.3	H11—C8—O13—C7	60.3	H11—C8—O13—C7	60.3

Table 2. Calculated harmonic (ω) and anharmonic (ν) frequencies of methyl propionate (in cm^{-1}) with corresponding A values ($cm\ mol^{-1}$) at MP2 level.

Method	DFT-PBEPBE		DFT-B3LYP		MP2		*A* value
Band assignment	Frequency (ω)	Frequency (ν)	Frequency (ω)	Frequency (ν)	Frequency (ω)	Frequency (ν)	
cCH3-rocking(?)	40	98	46	58	39	50	6.69E–21
cCH3-rocking(?)	120	48	130	51	148	142	4.58E–19
oCH3-rocking(?)	146	228	154	160	163	172	3.56E–19
COC bend(?)	200	285	207	212	211	215	3.67E–19
cCH3-rocking(?)	200	221	210	280	226	220	3.41E–19
COC bend(?)	319	330	330	334	338	362	3.10E–18
CCO bend(?)	435	433	445	442	452	446	1.06E–19
C=O wag	563	560	584	581	585	581	3.50E–19
OCO bend	635	624	656	665	664	666	5.61E–19
cCH3-rocking	785	779	817	809	816	811	1.34E–18
CCO Stretch	832	819	859	847	868	853	2.36E–18
O—CH3 stretch	961	935	979	955	1008	985	4.98E–19
CCO Stretch	1001	985	1031	1014	1048	1028	2.27E–18
CCO bend	1066	1040	1106	1082	1116	1092	3.50E–20
cCH3-rocking	1075	1048	1113	1088	1127	1098	1.85E–18
oCH3-rocking	1130	1109	1176	1150	1192	1167	2.12E–19
Skeletal def.	1153	1117	1201	1168	1214	1183	7.97E–18
Skeletal def.	1166	1134	1219	1179	1239	1202	5.28E–17
cCH3-twist	1238	1199	1286	1250	1293	1263	7.80E–21
CCO bend	1327	1286	1384	1345	1395	1357	1.49E–17
cCH3-wag	1366	1332	1423	1411	1424	1389	4.77E–19
CH2-bend	1408	1361	1466	1437	1474	1433	1.90E–18
oCH3-wag	1412	1379	1474	1449	1484	1449	2.55E–18
oCH3-rocking	1428	1390	1486	1445	1506	1465	1.35E–18
cCH3-rocking	1440	1416	1495	1485	1511	1487	1.18E–18
oCH3-scissoring	1446	1415	1501	1480	1518	1488	2.46E–18
cCH3-scissoring	1450	1408	1504	1483	1521	1493	1.30E–18
C=O stretch	1745	1713	1798	1766	1801	1771	2.89E–17
Sym-^{c}CH3-stretch	2975	2837	3038	2942	3092	3026	2.75E–18
Sym$^{\circ}$CH3+sym^{c}CH2	2979	2887	3045	3015	3096	2987	3.95E–18
Sym$^{\circ}$CH3+sym^{c}CH2	2986	2858	3049	3002	3097	3012	2.39E–18
Asym-^{c}CH2-stretch	3002	2843	3062	2910	3140	3000	3.45E–19
Asym^{c}CH3-stretch	3049	2899	3107	2980	3182	3046	2.60E–18
Asym-^{c}CH2-stretch	3056	2896	3114	2976	3186	3049	2.28E–18
Asym-$^{\circ}$CH2-stretch	3059	2900	3117	2969	3188	3048	2.86E–18
Asym-$^{\circ}$CH3-stretch	3087	2954	3150	3002	3221	3083	1.86E–18

angles are changing within 1–5°, thereby reconfirming our structure to be close to experimental values.

In Table 2, we present the harmonic and anharmonic IR frequencies obtained at DFT and MP2 levels of theory. In the mid- and higher IR frequency regions, we find that the MP2 gives larger frequency in comparison with DFT and therefore, the spectra obtained from MP2 level of theory are shown in Fig. 2(a).

Spectra recorded after methyl propionate deposition at 85 K (Fig. 2b) showed several peaks originating from the vibrations of the methyl propionate molecule as a result of interaction with IR photons. Many peaks were observed in the 4000–400 cm^{-1} region (Table 3) and are found to be in good agreement with the bands that are reported in the 654–1360 cm^{-1} region (Moravie & Corset 1974). Based on the values calculated, the peak positions observed 654, 807.7, 839 and 965.2 cm^{-1} are assigned to OCO bend, cCH_3 rocking, CCO stretching and O—CH_3 stretching vibrations, respectively. Another set of intense bands with peak positions at 1020.6, 1089, 1159 and 1180.5 cm^{-1} are assigned to CCO stretching, c—CH_3 rocking vibrations and the last two towards skeletal deformation, respectively. Next set of vibrational bands with peak positions at 1207, 1328, 1362.1, 1378.7, 1417.8, 1439.4 and 1461 cm^{-1} are assigned to cCH_3 twisting, CCO bend or skeletal deformation, cCH_3 wagging, CH_2 bending, oCH_3wagging, OCH_3 rocking and cCH_3 scissoring.

Other set of bands with peak positions at 1739.2, 2965.6, 2926.9/2951.7, 2982 and 3027.7 cm^{-1} are assigned to CO stretching, symmetric cCH_3 stretching, combination bands (originating from symmetric oCH_3 stretching + symmetric cCH_2 stretching), combination band and asymmetric oCH_3 stretching vibrations, respectively. However, several other peaks with peak positions at 854.2, 1262.7, 1284.7, 1507.2, 1804.4, 2848, 2883.7, 3453.7, 3524.5 and 3590 cm^{-1} are left unassigned. These bands may correspond to either overtone/combination bands or may even originate from the interaction between two methyl propionate molecules (dimers) (Hesse and Suhm 2009). The contribution from dimer molecules cannot be neglected as it is well known (Sivaraman et al. 2012, 2013) in such low-temperature molecular ices where the deposited parent molecule containing H, O and C atoms are known to have different sets of dimers (conformers).

Though there are several peaks that correspond to the methyl propionate molecule, the very intense peaks were observed at 1739.2 and 1159 cm^{-1}. The 1739.2 cm^{-1} corresponds to the CO stretch which might not be a unique feature to identify methyl propionate as CO stretch may arise from other molecules containing COO

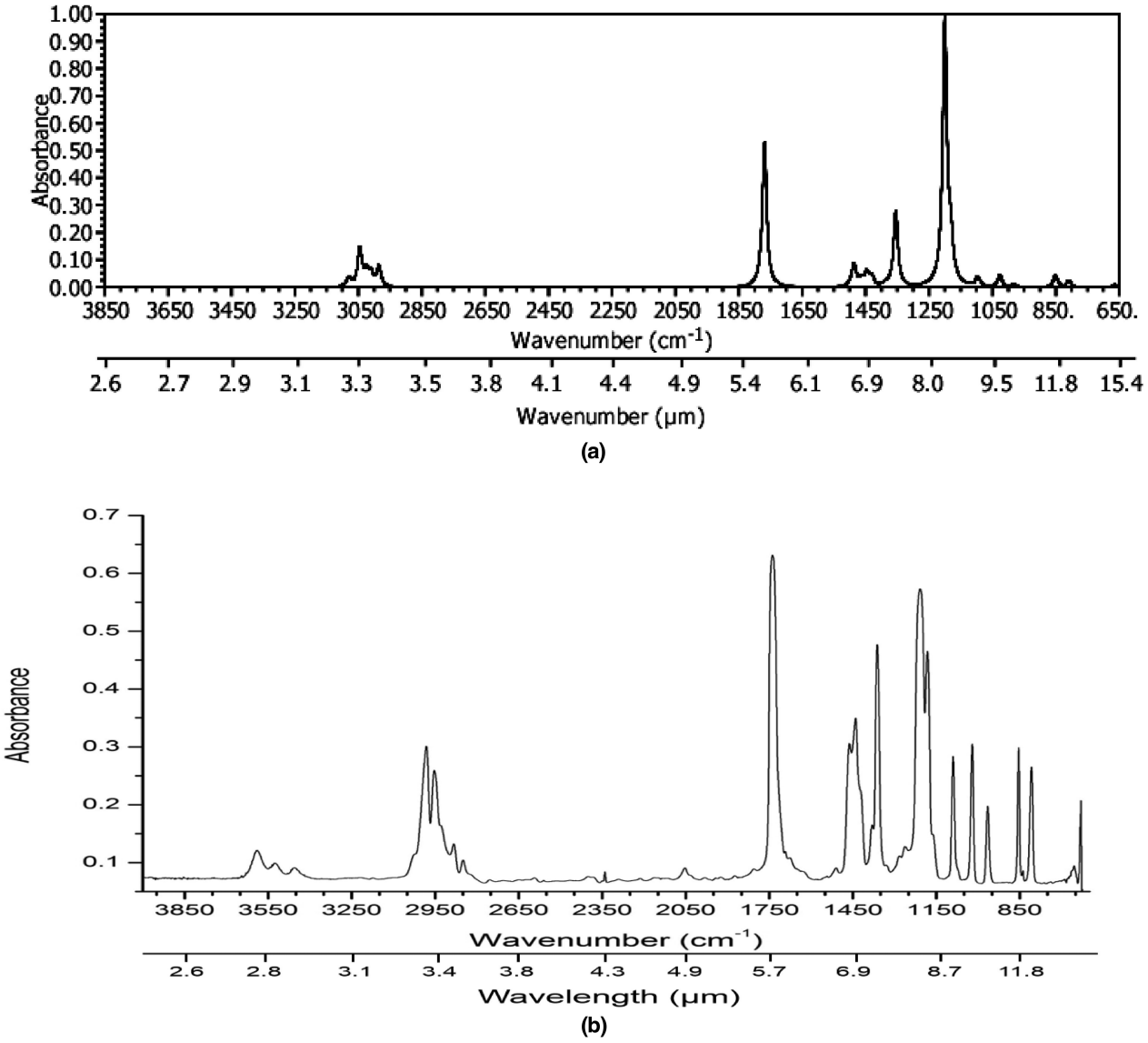

Figure 2. (a) Calculated infrared spectrum of methyl propionate in gas phase at MP2 level of theory. The IR spectrum has been displayed as a Lorentzian function with a half width at a half-maximum (HWHM) value of 8 cm^{-1} using the GABEDIT software (Allouche 2011). (b) Infrared spectrum of methyl propionate recorded after deposition at 85 K on to a ZnSe substrate.

group, such as methyl acetate, and the other very intense peak at 1159 cm^{-1} (8.62 μm) coincides with the intense and broad silicate bands. Identification even using the rest of the bands that may fall under the silicate 8–12 μm absorption may be difficult. We have to depend on the other peaks to identify this molecule in the cold regions of the interstellar region; in such a case, based on the IR spectra obtained experimentally a set of bands centring at 654 cm^{-1} (15.2 μm), 807.7 cm^{-1} (12.4 μm), 1362 cm^{-1} (7.3 μm), 1439 cm^{-1} (6.94 μm) and 2982 cm^{-1} (3.35 μm) can be used.

Chemical modelling for the formation of methyl propionate

In order to study the formation of methyl propionate in ISM, we develop a gas-grain chemical model. Our gas-phase chemical network contains the network of Woodall et al. (2007) and the network used in Das et al. (2013), Majumdar et al. (2013) and Majumdar, Das & Chakrabarti (2014). We also include a few new gas-phase reactions for the formation and destruction of methyl propionate and its related species. Our surface network mainly adopted from Das et al. (2013) and references therein. Our present gas-phase chemical network consists of 6160 reactions among 607 gas-phase species and present surface chemical network consists of 285 reactions. Gas-phase species are allowed to accrete on the grain surface. In order to mimic dense cloud condition, we consider, $n_H = 10^4$ cm^{-3}, $T = 10$ K and $A_V = 10$.

Gas-phase methyl propionate mainly forms through reactions between propionic acid (CH_3CH_2COOH) and methyl alcohol (CH_3OH) (reaction number 1). But the main challenge in chemical modelling is the unavailability of reaction pathways of its related species as well as required rate coefficients. For this, we prepare a complete reaction network for the formation and destruction of methyl propionate and its related species as shown in Table 4.

Table 3. Peak positions observed in the mid-IR spectrum of condensed methyl propionate at 85 K, under astrochemical conditions. Values in microns are given in bracket.

Wavenumber (cm^{-1})		
654 (15.3)	1262.7 (7.9)	1804.4 (5.5)
807.7 (12.4)	1284.7 (7.8)	2051.2 (4.9)
839 (11.9)	1328 (7.5)	2848 (3.5)
854.2 (11.7)	1362.1 (7.3)	2883.7 (3.5)
965.2 (10.4)	1378.7 (7.3)	2926.9 (3.4)
1020.6 (9.8)	1417.8 (7.1)	2951.7 (3.4)
1089 (9.2)	1439.4 (6.9)	2982 (3.4)
1159 (8.6)	1461 (6.8)	3027.7 (3.3)
1180.5 (8.5)	1507.2 (6.6)	3453.7 (2.9)
1207 (8.3)	1739.2 (5.7)	3524.5 (2.8)
		3590 (2.8)

Reaction number 1 is the main gas-phase production route of methyl propionate. But rate coefficient of this reaction is yet to be known. To this effect, we carried out quantum chemical calculation to find out rate coefficient of this reaction. We then find out the properties of this reaction. For this, we optimize the geometry of the reactants and products separately by using B3LYP functional with 6–311G++(d,p) basis set. It is noticed that the difference between total enthalpy of products and total enthalpy of reactants is −ve (i.e. the reaction is spontaneous in forward direction), so reaction number 1 is exothermic in nature. To compute reaction rate of reaction number 1, we use dispersive form of capture rate theory (Clary et al. 1994):

$$k_{\rm NN} = 8.56\ {\rm C_6^{1/3}}/\mu^{1/2}(K_{\rm B}\ T)^{1/6}{\rm cm^3\ mol^{-1}\ s^{-1}}, \qquad ({\rm R1})$$

where μ is collisional reduced mass, $K_{\rm B}$ is the Boltzmann constant and $C_6 = 3/2(E_aE_b/E_a + E_b)\ \alpha_a\alpha_b$, where, E_a and E_b are ionization potentials and α_a and α_b are the polarizabilities of CH_3OH and CH_3CH_2COOH, respectively. We use, $E_a = 10.85$ and $E_b = 10.525$ eV, and $\alpha_a = 3.29 \times 10^{-24}$ and $\alpha_b = 6.9 \times 10^{-24}$ cm^3 (Lide 2001). If all the parameters in equation (R1) are used in atomic units, then the factor 0.613×10^{-8} converts it into units of $cm^3\ mol^{-1}\ s^{-1}$ (Clary et al. 1994). Using all the parameters, we have the rate coefficient 1.16×10^{-8} $cm^3\ s^{-1}$ for the reaction number 1.

Propionic acid is the basic ingredient for the formation of methyl propionate in the gas phase. Following Blagojevic, Petrie & Bohme (2003), we use some ion-molecular reactions (reaction numbers 2–4) for the formation of propionic acid. Rate coefficients of these reactions were till date unknown. According to the discussion section of Majumdar et al. (2014) and references therein, Langevin collision rate ($k_{\rm L}$) formula could be used to compute rate coefficients of ion-neutral reactions, provided that neutrals are non-polar:

$$k_{\rm L} = 2\pi {\rm e\ sqrt}(\alpha d/\mu)\ {\rm cm^3\ s^{-1}}.$$

But in case of reaction numbers 2–4 (Table 4), both the neutrals (H_2O and CO) are polar in nature, so the situation would be different. Su & Chesnavich(1982) and Woon & Herbst (2009) used parameterized trajectory theory to compute the rate coefficients of this type of reactions. According to Woon & Herbst (2009), the Su-Chesnavich formula can be written in two different ways and both of which uses a parameter

$$x = \mu_{\rm D}/{\rm sqrt}\,(2\alpha {\rm K_B T})$$

where $K_{\rm B}$ is the Boltzmann constant, $\mu_{\rm D}$ is the dipole moment of the polar neutral species in Debye and T is the temperature in Kelvin. Depending on the values of 'x', rate coefficients could be parametrized by following two equations:

$$k_{\rm IN} = (0.4767x + 0.6200)\ k_{\rm L} \quad \text{for } x \geq 2,$$

$$k_{\rm IN} = [(x + 0.5090)2/10.526 + 0.9754]\ k_{\rm L} \quad \text{for } x < 2.$$

Note that for $x = 0$, above equations reduce to the Langevin expression. Following a similar approach, here also, we calculate the rate coefficients of these ion-polar reactions.

Methyl propionate is a stable molecule, but its related species could be destroyed by various mechanism, which could affect its production. Cationic species are mainly destroyed by the dissociative recombination (DR) reactions shown in Table 4. DR pathways for $C_2H_4CO^+$ (reaction number 5) and $C_2H_4CO^+H_2O$ (reaction number 6) are chosen by following the DR pathways of CH_2CO^+ (Woodall et al. 2007) and calculated by using following rate formula:

$$k_{\rm DR} = \alpha(T/300)^{\beta}\ \exp(-\gamma/T)\ {\rm cm^3\ s^{-1}},$$

where α , β and γ are the three constants. By following the rate constants used for CH_2CO^+, here also, we use $\alpha = 2 \times 10^{-7}$, $\beta = -0.5$ and $\gamma = 0$ for reaction numbers 5 and 6. DR pathways for $CH_3CH_2COOH^+$ (reaction number 7) have been assigned by following the DR pathways available for HCOOH (Woodall et al. 2007) and use $\alpha = 1.5 \times 10^{-7}$, $\beta = -0.5$ and $\gamma = 0$.

Propionic acid could be ionized by the interstellar photon. Following the reaction of HCOOH (Woodall et al. 2007), here we consider reaction number 8. Rate coefficient of this reaction is calculated by

$$k_{\rm PH} = \alpha\ \exp(-\gamma\ A_{\rm V})\ {\rm s^{-1}},$$

where $A_{\rm V}$ is the visual extinction parameter. For the dense cloud condition, we use $A_{\rm V} = 10$. For reaction number 8, we use

Table 4. Reactions for the formation and destruction of methyl propionate.

Reaction step	Type of reaction	Rate coefficient
1. $CH_3OH + CH_3CH_2COOH \rightarrow CH_3CH_2COOCH_3 + H_2O$	Neutral-neutral	1.16×10^{-8} $cm^3\ s^{-1}$
2. $C_2H_4^+ + CO \rightarrow C_2H_4CO^+$	Ion-molecular	3.47×10^{-10} $cm^3\ s^{-1}$
3. $C_2H_4CO^+ + H_2O \rightarrow C_2H_4CO^+H_2O$	Ion-molecular	1.105×10^{-8} $cm^3\ s^{-1}$
4. $C_2H_4CO^+H_2O + H_2O \rightarrow CH_3CH_2COOH + H_2O$	Ion-molecular	1.07×10^{-8} $cm^3\ s^{-1}$
5. $C_2H_4CO^+ + e^- \rightarrow C_2H_4 + CO$	Dissociative recombination	1.1×10^{-6} $cm^3\ s^{-1}$
6. $C_2H_4CO^+H_2O + e^- \rightarrow C_2H_4CO^+ + H_2O$	Dissociative recombination	1.1×10^{-6} $cm^3\ s^{-1}$
7. $CH_3CH_2COOH^+ + e^- \rightarrow C_2H_5 + CO + OH$	Dissociative recombination	8.21×10^{-7} $cm^3\ s^{-1}$
8. $CH_3CH_2COOH + PHOTON \rightarrow CH_3CH_2COOH^+ + e^-$	Photodissociation	2.0×10^{-10} s^{-1}
9. $CH_3CH_2COOH + CRPHOT \rightarrow C_2H_5 + CO + OH$	CRP	4.05×10^{-15} s^{-1}

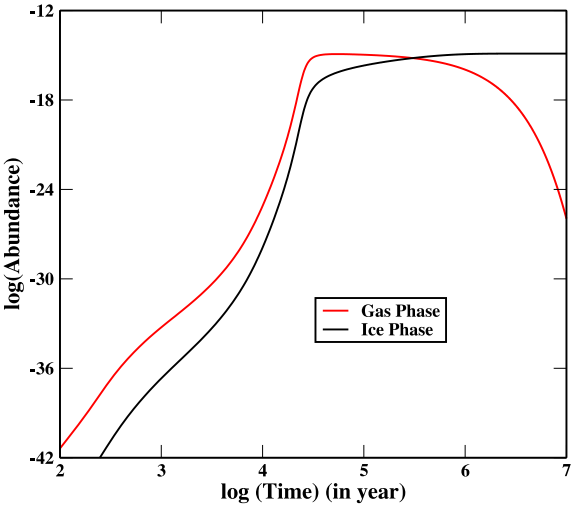

Figure 3. Time evolution of gas- and ice-phase methyl propionate in interstellar conditions.

$\alpha = 2.6 \times 10^{-10}$ and $\gamma = 2.6$ by following the pathways of HCOOH in Woodall et al. (2007).

Cosmic ray-induced photodissociation (CRP) effect also dissociate propionic acid. Reaction number 9 is considered here by following the photodissociation pathways of HCOOH (Woodall et al. 2007). Rate coefficient of reaction number 9 is calculated by

$$k_{\rm CR} = \alpha(T/300)^{\beta}\ \gamma/(1-\omega),$$

where ω is the dust grain albedo in the far ultraviolet (we use $\omega = 0.6$ and $T = 10$ K). For this reaction, we use $\alpha = 1.3 \times 10^{-17}$ and $\gamma = 124.5$ by following the pathways of HCOOH (Woodall et al. 2007).

In Fig. 3, we have shown the chemical evolution of methyl propionate in gas phase as well as in the ice phase. Here, we are not considering any formation or destruction pathways for the ice-phase methyl propionate. But since, we are considering the depletion of gas-phase species, interstellar grains could be populated by methyl propionate as well. Since no destruction pathways for the ice-phase methyl propionate are considered, it is achieving a steady state during the late stages. Abundance of gas-phase methyl propionate decreases, due to the destruction of its related species and depletion to the interstellar grain. From Fig. 3, we observe a peak abundance of methyl propionate with respect to total hydrogen nuclei to be 1.2×10^{-15} and 1.3×10^{-15}, respectively, for the gas and ice phase.

CONCLUSION AND IMPLICATIONS

Experimental IR spectra obtained showed several bands that corresponds to condensed methyl propionate at 85 K. Though there are several bands that shows the characteristic vibrations from methyl propionate molecule, it is only those bands falling on either side of the strong and broad silicate absorption that are presented in this paper can be used to detect its presence in the ISM. However, future experimental work to be carried out on methyl propionate ices in binary mixtures, such as methyl propionate / water, will help in identifying their coexistence on the icy mantles of cold dust grains. Experiment recording the IR spectra of methyl propionate as a function of temperature will be carried out as a separate spectroscopy study, which is beyond the scope of this manuscript, which will explain the nature of dimer formation, the phase transition and the present phase of methyl propionate at 85 K. Theoretical modelling strongly suggests the presence of methyl propionate molecules in the ice phase which will be a precursor for even larger and complex molecules.

ACKNOWLEDGEMENTS

BS would like to acknowledge Professor N. J. Mason, the Open University, UK and R. Mukherjee, PRL, Ahmedabad, India for their valuable discussions and comments in improving the quality of this manuscript. GG and MH would like to thank JST, CREST entitled 'Creation of Innovative Functions of Intelligent Materials in the basis of the Element Strategy'. AD and SKC want to thank ISRO Respond (grant no. ISRO/RES/2/372/11-12) and DST (grant no. SB/S2HEP-021/2013) project for their financial supports. LM wants to thank MOES for funding during this work. BS also thank INSPIRE grant (IFA- 11 CH -11).

REFERENCES

Allouche A.-R., 2011, J. Comput. Chem., 32, 174
Becke A. D., 1988, Phys. Rev. A, 38, 3098
Blagojevic V., Petrie S., Bohme D. K., 2003, MNRAS, 339, L7
Clary D. C., Haider H., Husain D., Kabir M., 1994, ApJ, 422, 7
Das A., Majumdar L., Chakrabarti S. K., Saha R., Chakrabarti S., 2013, MNRAS, 433, 3152
Frisch M. J. et al., 2009, Gaussian 09. Gaussian, Inc., Wallingford, CT, USA
Hesse S., Suhm M. A., 2009, Phys. Chem. Chem. Phys., 11, 11157
Karton A., Talbi D., 2014, Chem. Phys., 436, 22
Lee C., Yang W., Parr R. G., 1988, Phys. Rev. B, 37, 785
Lide D. R., 2001, in Lide D. R. ed., CRC Handbook of Chemistry and Physics, 82th ed., CRC Press, Boca Raton, FL
Majumdar L., Das A., Chakrabarti S. K., Chakrabarti S., 2013, New Astron., 20, 15
Majumdar L., Das A., Chakrabarti S. K., 2014, ApJ, 782, 73
Møller C., Plesset M. S., 1934, Phys. Rev., 46, 618
Moravie R. M., Corset J., 1974, Chem. Phys. Lett., 26, 210
Perdew J. P., Burke K., Ernzerhof M., 1996, Phys. Rev. Lett., 77, 3865
Sivaraman B., Raja Sekhar B. N., Jones N. C., Hoffmann S. V., Mason N. J., 2012, Chem. Phys. Lett., 554, 57
Sivaraman B., Raja Sekhar B. N., Nair B. G., Hatode V., Mason N. J., 2013, Spectrochim. Acta, 105, 238
Sivaraman B., Mukherjee R., Subramanian K. P., Banerjee S. B., 2014, Chem. Phys. Lett., 609, 167
Stephens P. J., Devlin F. J., Chabalowski C. F., Frisch M. J., 1994, J. Phys. Chem., 98, 11623
Strieter F. J., Templeton D. H., Scheuerman R. F., Sass R. L., 1962, Acta Crystallogr., 15, 1233
Su T., Chesnavich W. J., 1982, J. Chem. Phys., 76, 5183
Tercero B., Kleiner I., Cernicharo J., Nguyen H. V. L., López A., Caro G. M. M., 2013, ApJ, 770, L13
Venkateswarlu P., Gordy W., 1955, J. Chem. Phys., 23, 1200
Woodall J., Agúndez M., Markwick-Kemper A. J., Millar T. J., 2007, A&A, 466, 1197
Woon D. E., Dunning T. H., 1993, J. Chem. Phys., 98, 1358
Woon D. E., Herbst E., 2009, ApJS, 185, 273

This paper has been typeset from a Microsoft Word file prepared by the author.